Available online at www.sciencedirect.com

ScienceDirect

Advances in Space Research 70 (2022) 3220–3230

ADVANCES IN SPACE RESEARCH (a COSPAR publication)

www.elsevier.com/locate/asr

Influencing factors for the preparation of Fe^0 in lunar soil simulant using high-temperature carbothermic reduction

Yanhua Peng [a,b,c], Hong Tang [b,*], Bing Mo [b], Xiaojia Zeng [b], Bingkui Miao [a,*]

[a] Institution of Meteorites and Planetary Materials Research, Guilin University of Technology, Guilin 541006, China
[b] Center for Lunar and Planetary Sciences, Institute of Geochemistry, Chinese Academy of Sciences, Guiyang 550081, China
[c] Nanning College of Technology, Guilin 541006, China

Received 19 December 2021; received in revised form 9 July 2022; accepted 29 July 2022
Available online 3 August 2022

Abstract

Metallic iron (Fe^0) within lunar soil grains can affect their visual and near-infrared spectra, adhesion, biological toxicity, and electrostatic migration characteristics. The Fe^0 particle therefore is an important component of lunar soil. This study devised a high-temperature carbothermic reduction method for preparing Fe^0 via graphite reduction of Chinese Lunar Regolith Simulant (CLRS-2) in an argon atmosphere, which is similar to the Fe^0 in the agglutinitic glass of lunar samples. The X-ray diffraction and electron microscopy data show that the mixture of lunar soil simulants and graphite heated at high temperature rapidly quenched to form a glassy phase with dispersed Fe^0 particles, the microstructure of which is consistent with the α-Fe (bcc) in lunar soil. This paper also discusses the main influencing factors for preparing Fe^0, such as the ratio of raw materials, heating temperature, and holding time. The optimal experimental conditions are a graphite-to-CLRS-2 mass ratio of 1.0: 27.0 (Fe/C = 2.0: 2.6), reduction temperature of ~1600 °C, and holding time of ~4 h, which produce single-phase α-Fe with an average particle size of ~180 ± 10 nm and no residual impurities (e.g., graphite).

Keywords: Lunar soil simulant; Metallic iron; Carbothermic reduction; Influencing factors

1. Introduction

The lunar soil was formed in long-term space weathering, which involves micrometeorite impacts, solar wind particle bombardment, and cosmic ray radiation. Electron microscopy researches have shown that Fe^0 is an important product of the space weathering of lunar soil, and that it is widely contained within agglutinitic glass and distributed on rims of lunar soil grains (Basu et al., 2001; Housley et al., 1973). On the one hand, the space weathering on the lunar surface caused by solar wind and cosmic rays results in sputter deposits (Cain, 2010; Hapke, 2001; Keller and McKay, 1997). In bombardment by solar wind and cosmic rays, energetic particles can sputter and reduce Fe^{2+} from the superficial atomic layers of lunar soil grains to form Fe^0, which is then deposited on the outermost layer of the lunar soil grains (Burgess and Stroud, 2018; Keller and McKay, 1997). On the other hand, the high temperature generated by the high-speed impacts of micrometeorites can vaporize part of the lunar soil grains (Keller and Mckay, 1992; Keller and Mckay, 1993), which reduces gaseous Fe^{2+} to Fe^0. The Fe^0 particles are subsequently deposited on the surface of nearby lunar soil grains and covered by molten amorphous glass owing to the rapid cooling to the ambient temperature. The high temperature generated by the high-speed impacts of micrometeorites

* Corresponding authors.
E-mail addresses: pengyanhua188@163.com (Y. Peng), dongtianzhixing@163.com (H. Tang), mobing@mail.gyig.ac.cn (B. Mo), zengxiaojia@mail.gyig.ac.cn (X. Zeng), miaobk@glut.edu.cn (B. Miao).

https://doi.org/10.1016/j.asr.2022.07.074
0273-1177/

can also melt lunar soil and form silicate melts. In the high-vacuum environment of the Moon, part of the Fe^{2+} in silicate melt is reduced to Fe^0 (Basu et al., 2002; Housley et al., 1973; James et al., 2002; Liu et al., 2007). The Fe^0 particles are therefore wrapped by agglutinated glass that forms in rapid cooling of the silicate melt. Previous studies have suggested that Fe^0 particles contained within agglutinitic glass and distributed on rims of lunar soil grains have sizes of <1 μm (Morris, 1980), and are mostly tens to hundreds of nanometers in size (Hapke, 2001). Morris (1980) studied the Fe^0 content of various lunar soils using magnetization curves and ferromagnetic resonance. He concluded that typical lunar soil has about 0.54 ± 0.18 wt % Fe^0 and that highland lunar soils have somewhat less Fe^0 than maria regolith.

Analysis of Apollo samples showed that fine-grained lunar soil usually has higher Fe^0 content than lunar rocks by a factor of ~7.5–10 (Cain, 2010; Nagata et al., 1970), and that fine-grained lunar soils display extremely strong electrostatic and magnetic adhesion, electrostatic migration characteristics, low reflectivity, weak Fe^{2+} absorption intensity, and spectral redshift (Hapke, 2001; Liu et al., 2020; Liu et al., 2007; Pieters and Fischer, 1993). The Fe^0 particles in fine-grained lunar soil are typically nano-scale single-domain iron with superparamagnetic properties. Thus, superparamagnetic Fe^0 particles cause marked viscous magnetization of the lunar soil (Nagata et al., 1970). Furthermore, the presence of Fe^0 leads to a lower work function of fine-grained lunar soil. Photoemissions are therefore more likely to be generated in those lunar soil grains and charged under ultraviolet radiation on the lunar surface. Fe^0 particles are also known to have a significant effect on the lunar soil spectrum, leading to darkening and reddening of the spectrum and weakening of the characteristic absorption bands (Hapke, 2001).

Several methods have been tried to prepare Fe^0 from lunar soil simulants, such as microwave heating (Kelly and Rowson, 1995; Tang et al., 2012), laser irradiation, magnetron sputtering (Tang et al., 2012), plasma processing (Sen et al., 2010; Sen et al., 2011), porous silica gel powder reduction (Liu et al., 2007), and carbothermal reduction (Hung and McNatt, 2012). Previous studies have demonstrated that Fe^0 can be reduced when lunar soil simulant or iron-bearing minerals (e.g., ilmenite) are heated with carbon or graphite (Gupta et al., 1987; Gustafson et al., 2005; Hung and McNatt, 2012; Rice et al., 1996; Wang and Yuan, 2006). However, the main purpose of those studies was not the preparation of Fe^0 in lunar soil, but rather the kinetics and mechanism of the reduction process or the preparation of oxygen. The mixture of carbon and lunar soil simulant (or ilmenite) is heated at 850 °C to 1400 °C for 2 h, and the Fe^0 particles in the products are typically micron-sized or agglomerated (Hung and McNatt, 2012; Wang and Yuan, 2006). This is significantly different from the spherical submicroscopic metallic iron (SMFe) (Hapke, 2001) found in lunar soil. Apart from the significant differences in morphology of the Fe^0, the factors that influence the particle size and content of Fe^0 have not been discussed in the studies.

This study applies a carbothermic reduction method to reduce Fe^0 particles in lunar soil simulant CLRS-2 using graphite as the reductant. The requirements for the experiments are to ensure that no impurities are produced and that the Fe^0 prepared is closer in morphology, particle size, and content to the iron found in lunar soil. On the basis of the experiments, the main factors that affect the particle size and content of the Fe^0 in the preparation process were analyzed.

2. Materials and analytical methods

2.1. Basic principles

The principle of Fe^0 preparation using carbothermic reduction is that Fe-bearing materials are reduced to form Fe^0 particles using graphite as the reductant under high-temperature and low-oxygen fugacity conditions. The raw materials used in the experiments include high-titanium basaltic lunar soil simulant CLRS-2 developed by the Institute of Geochemistry, Chinese Academy of Sciences, and graphite as the reducing agent. The mineral composition of the CLRS-2 includes mainly basic volcanic glass, ilmenite, olivine, pyroxene, and plagioclase, and the chemical composition includes ~19.29 wt% Fe_2O_3 (Table 1). The reactions between the CLRS-2 and graphite during high-temperature heating are as follows:

$$FeO + C \rightarrow Fe + CO\uparrow \quad (1)$$

$$FeO + CO \rightarrow Fe + CO_2\uparrow \quad (2)$$

The total reaction is:

$$2FeO + C \rightarrow 2Fe + CO_2\uparrow \quad (3)$$

When heated to a temperature above 1200 °C, CLRS-2 melts completely and becomes a homogeneous silicate melt. FeO can be used to represent the Fe-bearing silicate melt. FeO reacts with graphite at high temperature to generate Fe^0 and carbon monoxide (Eq. (1)), and the carbon monoxide subsequently reacts with FeO to produce Fe^0 and carbon dioxide (Eq. (2)).

2.2. Experimental and analytical methods

The lunar soil simulant CLRS-2 and graphite were weighed according to a certain proportion (Table 2) and then placed in high-purity corundum crucibles and heated in a high-temperature atmospheric furnace. The temperature was raised to the range 1150–1600 °C at a rate of 10 °C/min and maintained for 0–4 h. An argon gas flow was continuously supplied during heating to maintain a low-oxygen-fugacity environment, which helped to reduce the Fe^0 particles. After heating, the samples were withdrawn from the furnace and cooled by quenching in water to obtain a silicate glass containing Fe^0 particles.

Table 1
Chemical composition of the lunar soil simulant CLRS-2 (wt%).

SiO_2	TiO_2	Al_2O_3	Fe_2O_3	MnO	MgO	CaO	Na_2O	K_2O	P_2O_5	Ignition loss	Total
40.64	6.79	12.07	19.29	0.22	7.68	9.50	2.26	0.83	0.19	0.50	99.97

Table 2
Raw material ratios and experimental conditions in this study.

Sample	mass ratio (C/CLRS-2)	molar ratio (Fe/C)	experimental conditions heating temperature(℃)/holding time(h)
R1	1.0: 39.0	2.0: 1.8	1600/4.0
R2	1.0: 27.0	2.0: 2.6	1150/2.0, 1200/2.0, 1300/2.0, 1400/2.0, 1500/2.0, 1600/0, 1600/1.5, 1600/2.0, 1600/2.5, 1600/3.0, 1600/3.5, 1600/4.0
R3	1.0: 23.0	2.0: 3.0	1600/4.0

The polished sections for scanning electron microscopy (SEM) and micro-X-ray diffractometer (μ-XRD) analysis were cut from the middle of the quenched sample, with the plate surface perpendicular to the bottom of the crucible and cut parallel to the long side of the crucible.

The in-situ determination of crystalline phases in the reduced sample were investigated using a Rigaku Dmax Rapid V micro-X-ray diffractometer (μ-XRD) at the Guangzhou Institute of Geochemistry, Chinese Academy of Sciences (CAS). The operating conditions of the diffractometer were 40 kV and 30 mA, using a 100 μm type collimator and an exposure time of 100 s for the analysis. The powder crystal X-ray diffraction (XRD) analysis were completed at the Institute of Geochemistry, CAS, Guiyang.

The morphology, content, particle size distribution and elemental composition of Fe^0 particles in polished sections were studied using an FEI Scios Dual Beam scanning electron microscope (SEM) housed in the Institute of Geochemistry, CAS, Guiyang. Back-scattered electron (BSE) images were obtained in high vacuum, at an accelerating voltage of 15 kV and a working distance of ~7 mm from sample to target.

Furthermore, the samples were cut into an ultrathin section using a focused ion beam (FIB) and analyzed using a transmission electron microscope (TEM) equipped with an energy dispersive spectrometer (EDS). Chemical nano-analysis of FIB samples was obtained by EDS and the microstructure of iron was obtained by high resolution (HR) TEM images and selected area electron diffraction (SAED) patterns.

To explore the effect of high-temperature carbothermic reduction of lunar soil simulant on preparing Fe^0, this study mainly evaluated the size distribution and area percentage of Fe^0 particles (referred to as content). Both the size and content can be obtained from the SEM image statistics using ImageJ software.

3. Results and discussion

3.1. Characteristics of Fe^0

The Fe^0 within lunar soil is α-Fe with body-centered cubic (bcc) structure (Liu et al., 2007; Thompson et al., 2015). Both the diffraction peak shape and high diffraction intensity in the XRD pattern (Fig. 1) show that the α-Fe is produced in the sample with a graphite/CLRS-2 mass ratio of 1.0: 27.0 (Fe/C = 2.0: 2.6) reduced at 1600 °C for 4 h. EDS also shows that the white dots dispersed in the prepared section (Fig. 2a) is elemental iron (Fig. 2b). To gain further insight into the characteristics of the iron-rich particles, we examined them through a high-angle annular dark field (HAADF). The result shows that the particles are typically spherical, the same as those of Fe^0 in lunar soil (Basu, 2005), with a diameter of approximately 180 nm (Fig. 2c), and that this particle size is distributed within the range < 1 μm for Fe^0 in lunar soils (Basu, 2005; Basu et al., 2001; Morris, 1980). A high-resolution (HR) TEM image and selected area electron diffraction (SAED) pattern (Fig. 2d and 2e) show a lattice plane distance of 0.202 nm for the Fe^0 particle, which is close to Tang et al.'s (2017) 0.204 nm and Thompson et al., (2015) 0.203 nm. All of these analytical techniques confirm that the iron in the product is α-Fe. Furthermore, the μ-XRD pattern (Fig. 1) shows no notable impurity peaks, which implies that no graphite reductant residue and/or other impurity phases were generated during this experiment.

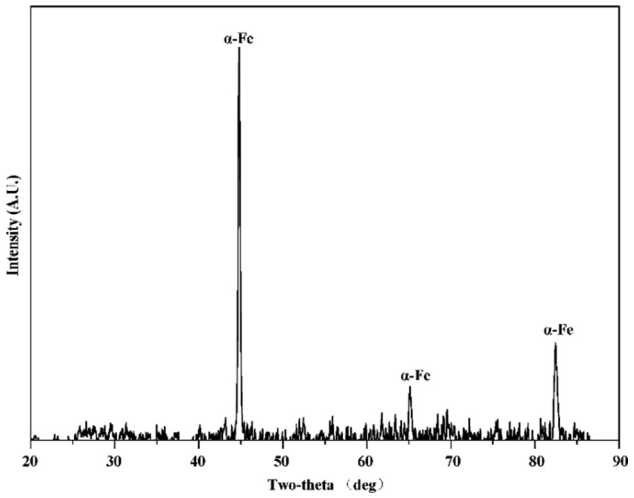

Fig. 1. μ-XRD pattern of a sample with a graphite/CLRS-2 mass ratio of 1.0: 27.0 (Fe/C = 2.0: 2.6) reduced at 1600 °C for 4 h. Single-phase α-Fe is produced.

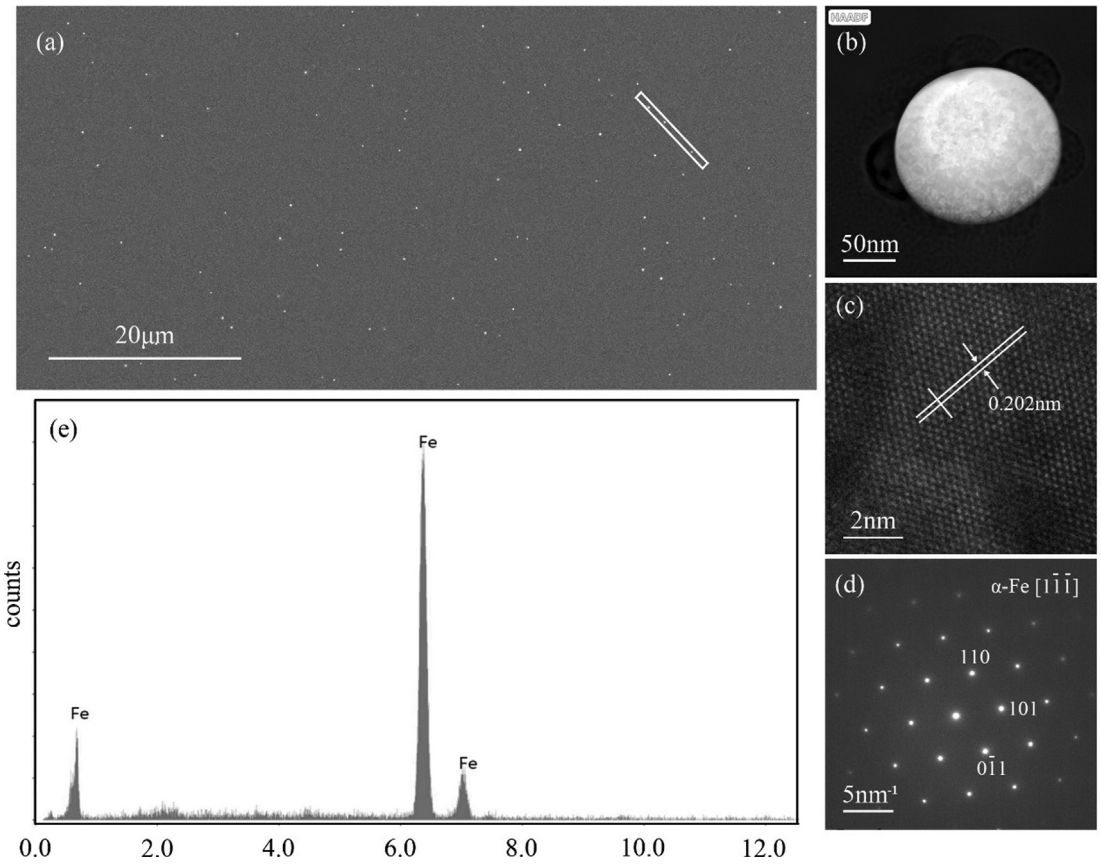

Fig. 2. SEM and TEM results. (a) BSE image of the reduced sample. The white rectangle indicates the extraction location of the foil for the focused ion beam (FIB). (b) HAADF image of a spherical Fe^0 particle. (c) HR image and (d) SAED pattern of the Fe^0 in the sample, which is indexed as α-Fe (bcc). (e) EDS result for the Fe^0 particle in (b).

3.2. Analysis of influencing factors

Analysis of the experimental products indicates that the Fe^0 characteristics are sensitive to the preparation conditions (Francis and El-Midany, 2008). The Fe^0 content and particle size are mainly affected by three factors: raw material ratio, heating temperature, and holding time.

3.2.1. Influence of raw material ratios

A spherical metal iron ball is observed at the bottom of the crucibles of the three samples heated at 1600 °C for 4 h, which indicates Fe^0 particle aggregation during the reduction process (Fig. 3). Sample R3 also shows a small amount of graphite residue on its surface, whereas none is visible on samples R1 and R2 and not even detected in their XRD patterns (Fig. 1). This indicates that the amount of graphite was excessive in sample R3 but not in samples R1 and R2.

The Fe^0 content and particle size of the samples are estimated from five representative BSE images (Fig. 4). The statistical results are listed in Table 3. The Fe^0 content in sample R3 is 0.09 ± 0.01 vol%, which is significantly higher than those of samples R1 (0.01 ± 0.01 vol%) and R2 (0.06 ± 0.02 vol%). Furthermore, the average particle size in sample R3 is 0.40 ± 0.07 μm, which is generally larger than in samples R1 (0.13 ± 0.02 μm) and R2 (0.18 ± 0.01 μm).

The results indicate that the Fe^0 content and particle size increase with decreasing Fe/C ratio (Fig. 5). A higher graphite ratio leads to a larger contact area between the reaction materials and facilitates the reaction; thus, more Fe^0 is produced. When the number of small Fe^0 particles distributed in the melt increases, the aggregation probability and particle size increase. In sample R3, the graphite was retained as an impurity because the ratio was too high (Fe/C = 2.0: 3.0), while in sample R1 the graphite ratio was too low (Fe/C = 2.0: 1.8), resulting in a low Fe^0 content as well. R2 did not have excess graphite, and its Fe^0 particles are similar in size to those of R1 and are more abundant. To obtain a certain amount of Fe^0 particles with a size closer to that in lunar soil and free of impurities, R2 with an Fe/C molar ratio of 2.0: 2.6 is recommended for preparing Fe^0 in such an experiment.

3.2.2. Influence of heating temperature

Previous studies have shown that the melting temperature of basalts of different mineral compositions range from 1175 to 1500 °C (Chen et al., 2017; Dzhigiris et al., 1983; Makhova et al., 1989). In this study, when R2 was treated at a heating temperature of 1150 °C, the products remaining were plagioclase, pyroxene, olivine, ilmenite, and magnetite, with no α-Fe, as shown by the powder crys-

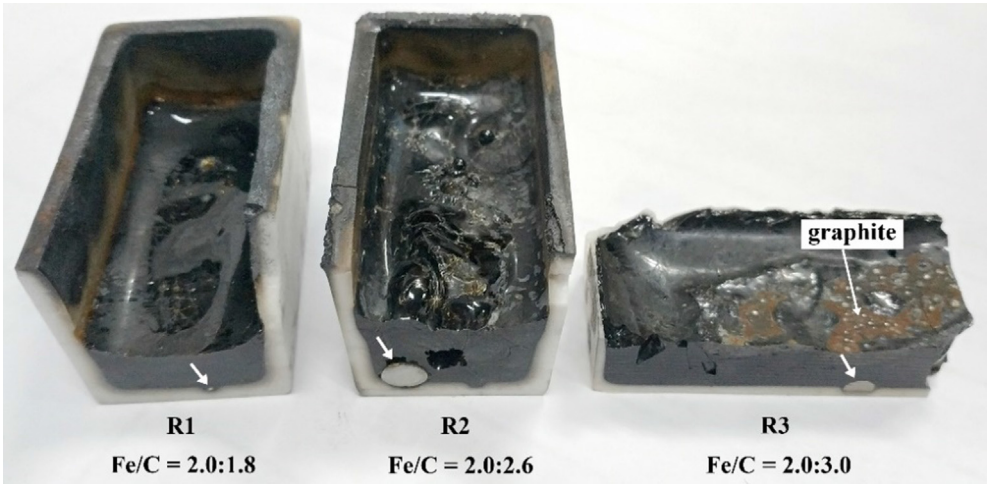

Fig. 3. Hand specimens of samples reduced at 1600 °C for 4 h with varying raw material ratios. The short arrows indicate a deposited metal iron ball. Residual graphite is found on the surface of sample R3.

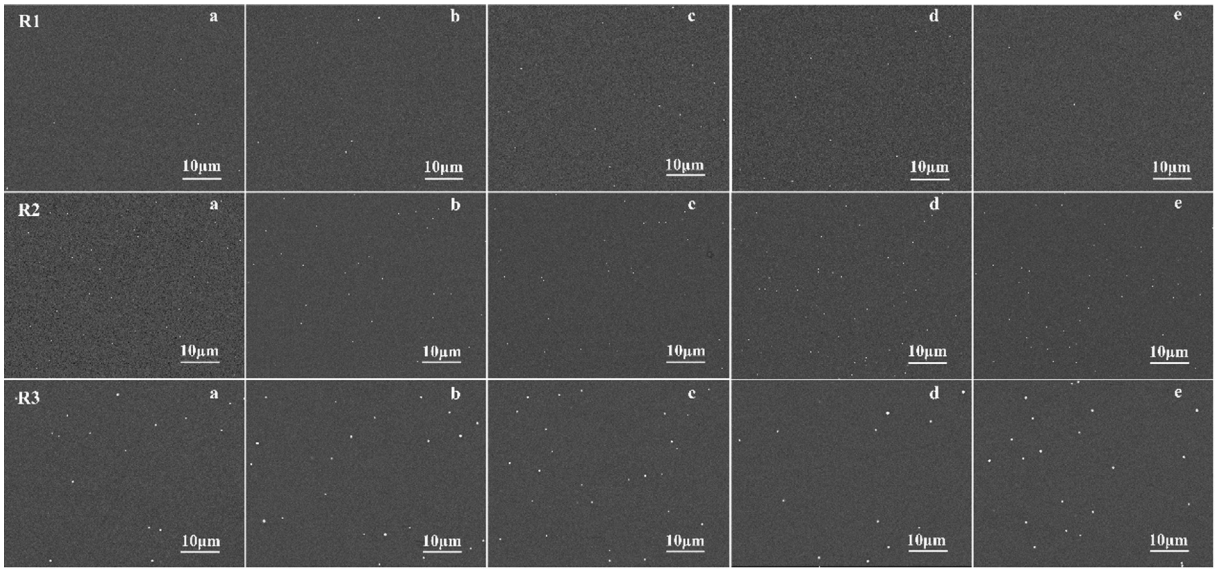

Fig. 4. BSE images of R1–R3 reduced at 1600 °C for 4 h. Rows 1–3 show samples R1–R3 with different raw material ratios, respectively. (a)–(e) correspond to five respective symmetrical parts of the polished section of the sample. The white dots are Fe^0 particles.

Table 3
Statistics of Fe^0 content and particle size based on BSE images of R1-R3 heated at 1600℃ for 4 h.

Images	R1		R2		R3	
	vol%	D/μm	vol%	D/μm	vol%	D/μm
a	<0.01	0.12	0.04	0.18	0.09	0.37
b	0.01	0.12	0.05	0.19	0.08	0.36
c	0.01	0.12	0.04	0.18	0.08	0.33
d	0.02	0.17	0.08	0.19	0.10	0.51
e	0.01	0.14	0.06	0.18	0.11	0.41
Avg.	0.01 ± 0.01	0.13 ± 0.02	0.06 ± 0.02	0.18 ± 0.01	0.09 ± 0.01	0.40 ± 0.07

The statistical data exclude the metal iron balls that aggregated and settled at the bottom of the crucible; vol%: Fe^0 area percentage; D: Fe^0 diameter. a-e correspond to the image labels.

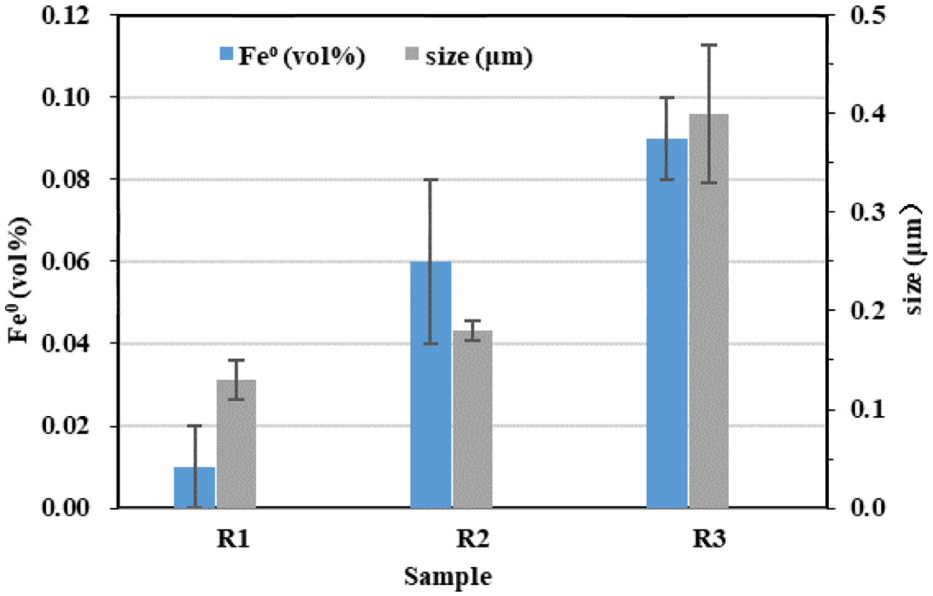

Fig. 5. Distributions of the average Fe^0 content and particle size in the samples heated at 1600 °C for 4 h with varying raw material ratios.

tal X-ray diffraction analysis (XRD) pattern (Fig. 6a) and BSE images of the crystal morphology (Fig. 6b). This suggested that, in this study, the raw material did not melt completely and no Fe^0 was reduced when heated to 1150 °C.

Although there was also no clear α-Fe peak in the XRD pattern of R2 heated at 1200 °C (Fig. 7), all of the minerals melted and a silicate glass formed. Fe^0 particles are clearly observed in the BSE images of all of the samples reduced at temperatures above 1200 °C (Fig. 8). No α-Fe was detected in the XRD pattern of R2 reduced at 1200 °C, probably because its content was below the detection limit. It is noteworthy that small precipitated iron balls were found at the bottom of the crucible when R2 was heated at 1600 °C for 2 h, but not when it was heated at 1200–1500 °C for 2 h.

Figs. 8 and 9 and Table 4 show that when R2 was heated at 1200–1600 °C for 2 h, the Fe^0 content and particle size initially increase with increasing heating temperature, from relatively low values of 0.03–0.05 vol% and 0.72–0.67 μm, respectively, at low temperature (1200–1300 °C) to substantially higher values of 0.72–1.95 vol% and 6.48–9.03 μm at 1400–1500 °C, and then decrease to 0.78 ± 0.43 vol% and 4.23 ± 1.13 μm upon heating to 1600 °C. Studies have shown that increasing heating temperature can help improve the reductive degree and rate of the reduction of iron-bearing minerals (Francis and El-Midany, 2008; Wang and Yuan, 2006). Thus, the trend in Fig. 9, where the average Fe^0 content and particle size increases and then decreases with rising heating temperature, can be explained as follows. The reduction ability at 1200–1300 °C is relatively weak owing to the low temperature, and the Fe^0 content is thus low. The low Fe^0 content and high melt viscosity at low temperature naturally reduce the probability of Fe^0 particle aggregation, which results in

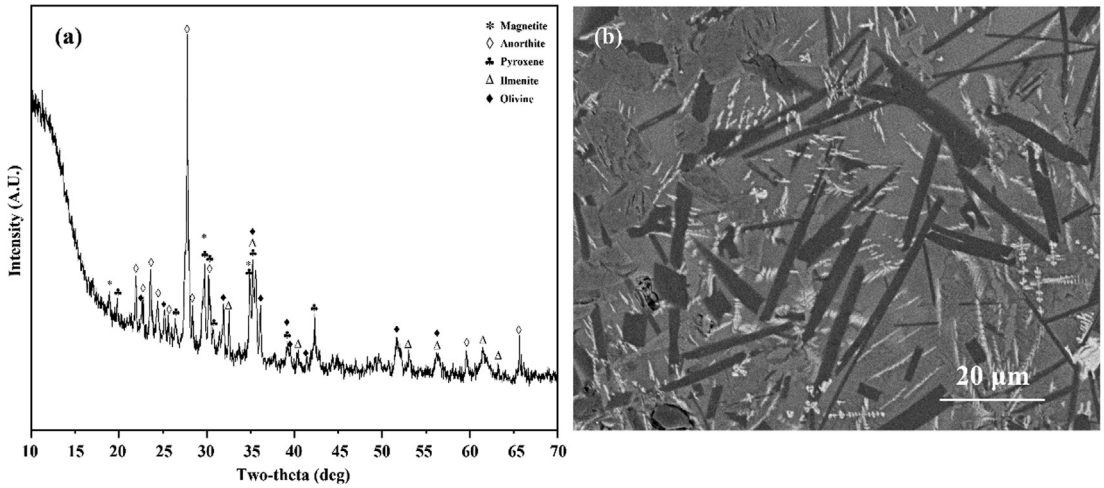

Fig. 6. XRD pattern (a) and BSE image (b) of R2 heated at 1150 °C for 2 h.

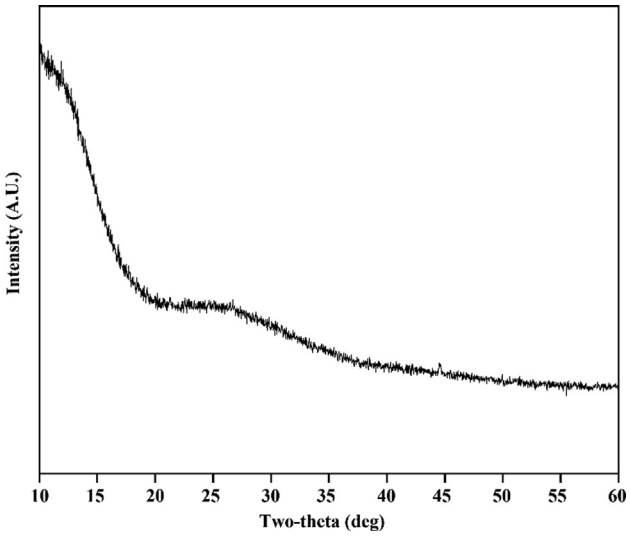

Fig. 7. XRD pattern of R2 heated at 1200 °C for 2 h.

smaller Fe^0 particles. The Fe^0 content and probability of Fe^0 particle agglomeration increase upon increasing the temperature to 1400–1500 °C, thus resulting in a larger average particle size. The large standard deviations of the retrieved values at 1400–1500 °C reflects a wide range of Fe^0 particle sizes, which indicates that the reduction and aggregation of the Fe^0 particles occurred simultaneously. As an increasing number of Fe^0 particles aggregate and grow to a certain size, they will tend to settle owing to gravity, as shown in the samples heated at 1600 °C in which small iron balls were deposited at the bottoms of the crucibles (Table 4). Aggregate deposition significantly reduces the Fe^0 particle content remaining in the melt, as well as the average Fe^0 particle size of the retained Fe^0 particles. The results indicate that higher temperatures are more conducive to Fe^0 reduction but also enlarge the Fe^0 particle size prior to deposition of the iron aggregate balls.

3.2.3. Influence of holding time

When R2 was heated at 1600 °C for various times, small metal balls settled at the bottom of the crucible in the samples that were kept at this temperature for 1.5, 2.0, 2.5, 3.0, 3.5, and 4.0 h, except for the sample that was quenched immediately upon heating to 1600 °C (Table 5). To meet the need for small Fe^0 particles and well evaluate the efficiency of Fe^0 production, these iron balls are not included in the statistical analysis. Figs. 10 and 11 and Table 5 show the change in Fe^0 content and particle size with increasing holding time at a reduction temperature of 1600 °C, starting from 0.22 ± 0.16 vol% and 1.16 ± 0.98 μm, respectively, in the sample quenched immediately after heating

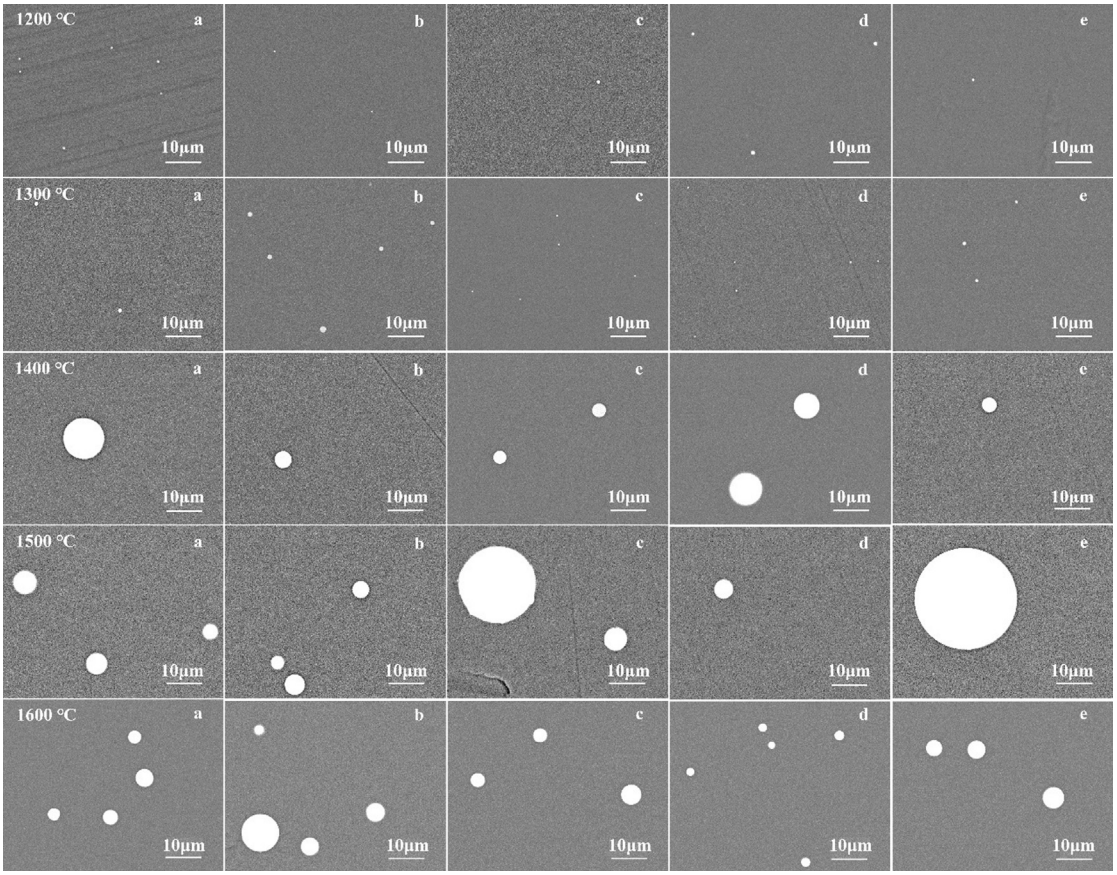

Fig. 8. BSE images of R2 heated at 1200–1600 °C for 2 h. Rows 1–5 show heating temperatures of 1200, 1300, 1400, 1500, and 1600 °C, respectively. (a)–(e) correspond to five respective symmetrical parts of the polished section of the sample. The white dots are Fe^0 particles.

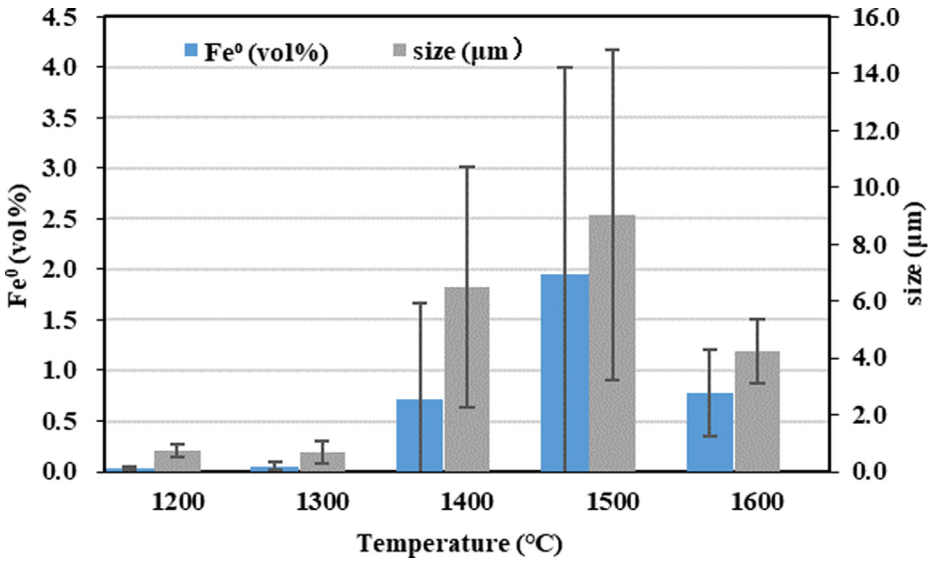

Fig. 9. Distributions of average Fe^0 content and particle size when R2 was heated at 1200–1600 °C for 2 h.

Table 4
Statistics of Fe^0 content and particle size based on BSE images of R2 heated at 1200-1600℃ for 2 h.

Heating temperature	vol%					Avg.	D/μm					Avg.
	a	b	c	d	e		a	b	c	d	e	
1200 °C	0.03	0.02	0.05	<0.01	0.04	0.03 ± 0.02	1.08	0.47	0.72	0.72	0.60	0.72 ± 0.23
1300 °C	0.03	0.02	0.02	0.11	0.05	0.05 ± 0.04	1.05	0.43	0.36	0.37	1.12	0.67 ± 0.38
1400 °C	0.14	0.19	0.78	0.16	2.35	0.72 ± 0.95	4.67	3.87	11.25	1.93	10.67	6.48 ± 4.22
1500 °C	0.40	3.06	0.57	5.05	0.70	1.95 ± 2.04	4.50	13.74	5.35	16.80	4.76	9.03 ± 5.81
1600 °C*	0.52	1.05	1.37	0.68	0.30	0.78 ± 0.43	4.40	5.28	5.07	3.93	2.44	4.23 ± 1.13

* Metallic iron balls aggregated and settled at the bottom of the crucible. The statistical data do not include the iron balls.

Table 5
Statistics of Fe^0 content and particle size based on BSE images of R2 heated at 1600℃ for 0–4.0 h.

Holding time	vol%					Avg.	D/μm					Avg.
	a	b	c	d	e		a	b	c	d	e	
0 h	0.15	0.34	0.16	0.03	0.44	0.22 ± 0.16	1.97	0.48	0.46	0.43	2.45	1.16 ± 0.98
1.5 h*	0.03	0.49	0.35	0.43	0.07	0.27 ± 0.20	5.39	5.13	5.30	0.62	0.69	3.43 ± 2.53
2.0 h*	0.52	1.05	1.37	0.68	0.30	0.78 ± 0.43	4.40	5.28	5.07	3.93	2.44	4.22 ± 1.13
2.5 h*	0.52	0.78	0.50	0.85	0.56	0.64 ± 0.16	3.42	2.28	3.25	2.75	2.64	2.87 ± 0.46
3.0 h*	0.13	0.09	0.06	0.14	0.12	0.11 ± 0.03	0.48	0.49	0.44	0.41	0.52	0.47 ± 0.04
3.5 h*	0.07	0.05	0.09	0.09	0.12	0.08 ± 0.02	0.38	0.19	0.29	0.28	0.34	0.29 ± 0.07
4.0 h*	0.04	0.05	0.04	0.08	0.06	0.06 ± 0.02	0.18	0.19	0.19	0.19	0.18	0.18 ± 0.01

* Metallic iron balls aggregated and settled at the bottom of the crucible. The statistical data do not include the iron balls.

to 1600 °C. These values initially increase with increasing holding time to maxima of 0.78 ± 0.43 vol% and 4.22 ± 1.13 μm after being held for 2 h, remain relatively constant upon increasing the heating duration to 2.5 h, and then abruptly decrease, reaching minima of 0.06 ± 0.02 vol% and 0.18 ± 0.01 μm after being held for 4 h.

The experiments show that small iron balls were deposited in the samples with holding times of 1.5–4 h, and the Fe^0 content increased with increasing holding time when it was <2.5 h (Table 5 and Fig. 11). It is generally accepted that the ilmenite reduction process with carbon can be divided into three stages: an early stage with a quick reduction rate, a middle stage with the reduction time prolonged, and a stage where the reaction rate decreases and the reaction is finally arrested (Wang and Yuan, 2006). In this paper, we therefore consider that the Fe^0 reduction rate is very high and higher than the aggregation rate during the first 2.5 h. The Fe^0 content drops rapidly when the holding time is 3.0 h, and then it decreases slowly (Fig. 10). This can be explained by the large amount of Fe^0 particles that aggregate and deposit, which subsequently reduces the amount of small Fe^0 particles retained in the melt. For holding times longer than 3.0 h, the rates of aggregation and sedimentation are likely the highest,

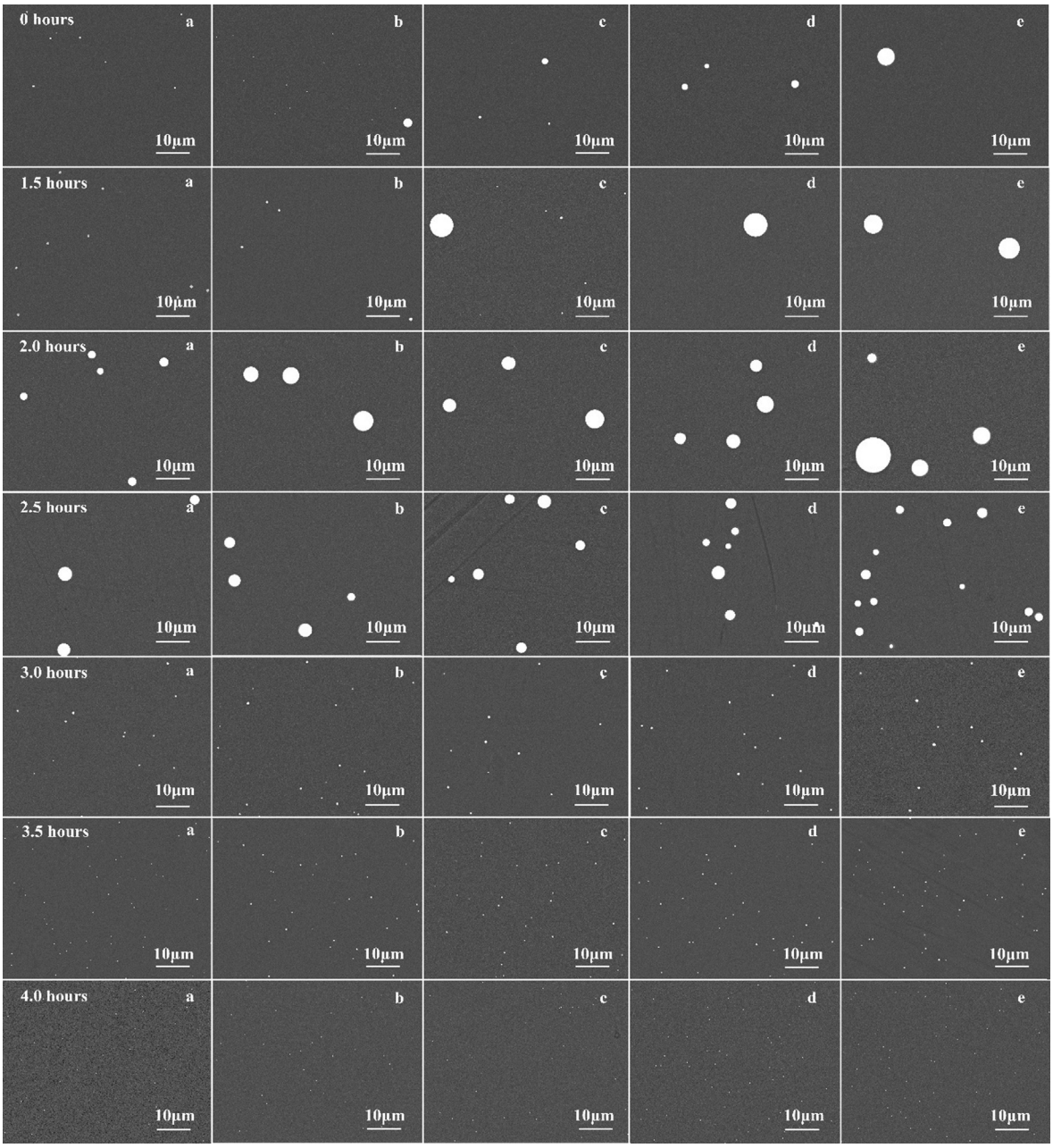

Fig. 10. BSE images of R2 heated at 1600 °C for different holding times. Rows 1–7 show holding times of 0, 1.5, 2.0, 2.5 3.0, 3.5, and 4.0 h, respectively. (a)–(e) correspond to five respective symmetrical parts of the polished section of the sample. Note that the most dramatic transition occurs between holding times of 2.5 and 3 h.

which is reflected by the lower Fe^0 content and particle size in the melt (Table 5).

In summary, the raw material ratio, heating temperature, and holding time have a significant effect on the Fe^0 content and particle size when using carbothermic reduction to prepare Fe^0 in lunar simulant. A low Fe/C ratio and high temperature are conducive to iron reduction. The Fe^0 particle size shows a negative correlation with the Fe/C ratio. Increasing the graphite content in raw materials not only increases the Fe^0 particle size, but also leads to impurities in the product when the graphite is excessive. High temperature is more conducive to Fe^0 reduction but also enlarges the Fe^0 particle size prior to deposition of the iron aggregate balls. Theoretically, a longer holding time leads to a higher reaction degree and more Fe^0 reduction. However, the reduced Fe^0 particles also tend to aggregate and grow over time. When the Fe^0 particles grow sufficiently large, they sink and deposit at the bottom of the crucible, thus reducing the content and particle size of the Fe^0 retained in the melt. A reasonable holding time is therefore important for controlling the Fe^0 content and particle size. When a sample with a graphite/CLRS-2 mass ratio of 1.0:27.0 is heated at 1600 °C for ~4 h, the average Fe^0 particle size and content

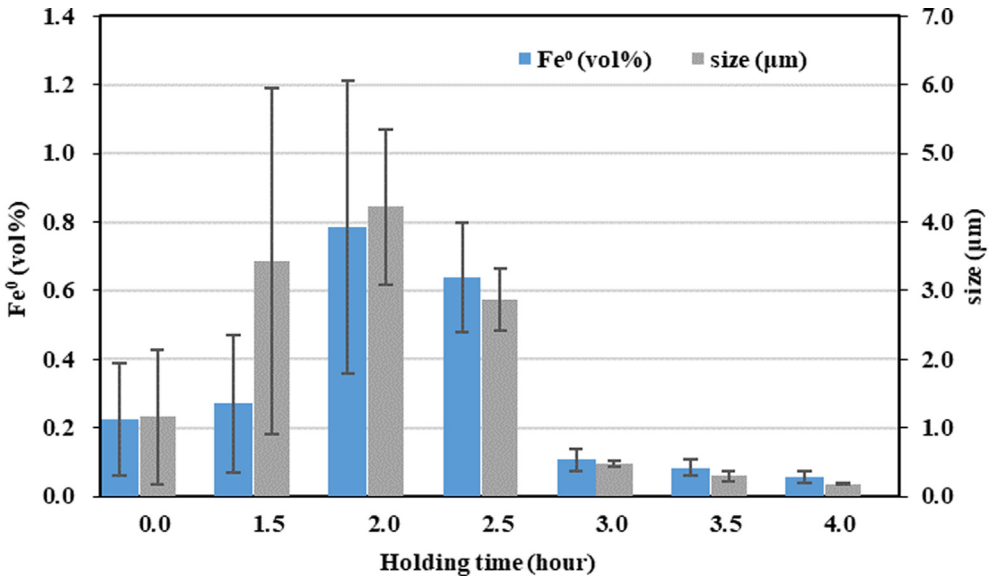

Fig. 11. Average Fe^0 content and particle size distributions in the product as functions of holding time when R2 is heated at 1600 °C.

are ~180 ± 10 nm and 0.06 ± 0.02 vol%, respectively. This Fe^0 content is lower than the average percentage of Fe^0 in lunar soils (0.54 ± 0.18 wt%) from the Morris (1980) study, but can be enriched by magnetic separation at a later stage. This Fe^0 particle size is within the range for Fe^0 in lunar soils (<1 μm), but it is still slightly coarser than the average particle size (~90 ± 7 nm). Further work is needed to address this to obtain a more compliant Fe^0 particle.

4. Conclusions

The experiments of this study suggest that high-temperature carbothermic reduction can be used to manufacture Fe^0 in lunar soil simulant. BSE and HAADF images show that the Fe^0 particles in the reduced sample are spherical. The Fe^0 particle structure has been confirmed as α-Fe by a high-resolution TEM image and SAED pattern. The experimental results clearly indicate that the raw material ratio, heating temperature, and holding time significantly affect the prepared Fe^0 content and particle size in lunar soil simulant. Under the conditions of a graphite/CLRS-2 mass ratio of 1.0:27.0 (Fe/C = 2.0:2.6), heating temperature of ~1600 °C, and holding time of ~4 h, the average Fe^0 particle size and content are approximately 180 nm and 0.06 vol% with no residual impurities. More research is required in the future to obtain Fe^0 that better matches the iron in lunar soil and better meets the needs of current scientific research and engineering tests.

Declaration of Competing Interest

The authors declare that they have no known competing financial interests or personal relationships that could have appeared to influence the work reported in this paper.

Acknowledgments

This research was supported by the B-type Strategic Priority Program of the Chinese Academy of Sciences (No. XDB41000000), National Natural Science Foundation of China (Nos.41931077), Pre-research project on Civil Aerospace Technologies by CNSA (No. D020201), Youth Innovation Promotion Association CAS (2018435), Guangxi University Young and middle-aged teachers' basic scientific research ability improvement project (No. 2020KY58009), Guangxi Scientific Base and Talent Special Projects (No. AD1850007).

References

Basu, A., 2005. Nanophase Fe 0 in lunar soils. J. Earth Syst. Sci. 114 (3), 375–380.
Basu, A., Wentworth, S.J., Mckay, D.S., 2001. Occurrence and Distribution of Feo-Globules in Lunar Agglutinates. Lunar Planet. Sci. XXXII.
Basu, A., Wentworth, S.J., McKay, D.S., 2002. Heterogeneous agglutinitic glass and the fusion of the finest fraction (F3) model. Meteorit. Planet. Sci. 37, 1835–1842.
Burgess, K., Stroud, R., 2018. Coordinated nanoscale compositional and oxidation state measurements of lunar space-weathered material. J. Geophys. Res. Planets 123 (8), 2022–2037.
Cain, J.R., 2010. Lunar dust: The Hazard and Astronaut Exposure Risks. Earth Moon Planet. 107 (1), 107–125.
Chen, X., Zhang, Y., Hui, D., Chen, M., Wu, Z., 2017. Study of melting properties of basalt based on their mineral components. Compos. B Eng. 116, 53–60.
Dzhigiris, D.D., Makhova, M.F., Gorobinskaya, V.D., Bombyr', L.N., 1983. Continuous basalt fiber. Glass Ceram. 40 (9), 467–470.
Francis, A., El-Midany, A., 2008. An assessment of the carbothermic reduction of ilmenite ore by statistical design. J. Mater. Process. Technol. 199 (1–3), 279–286.
Gupta, S.K., Rajakumar, V., Grieveson, P., 1987. Kinetics of reduction of ilmenite with graphite at 1000 to 1100 C. Metall. Trans. B 18 (4), 713–718.

Gustafson, R.J., Rice, E.E., White, B.C., 2005. Carbon reduction of lunar regolith for oxygen production. In: AIP Conference Proceedings. American Institute of Physics, pp. 1224–1228.
Hapke, B., 2001. Space weathering from Mercury to the asteroid belt. J. Geophys. Res. Planets 106 (E5), 10039–10073.
Housley, R.M., Grant, R.W., Paton, N.E., 1973. Origin and characteristics of excess Fe metal in lunar glass welded aggregates. In: Lunar and Planetary Science Conference Proceedings, p. 2737.
Hung, C.-C., McNatt, J., 2012. Lunar dust simulant containing nanophase iron and method for making the same. Google Patents.
James, C., Letsinger, S., Basu, A., Wentworth, S., McKay, D., 2002. Size Distribution of Fe^0 Globules in Lunar Agglutinitic Glass. In: Lunar and Planetary Science Conference, p. 1827.
Keller, L.P., Mckay, D.S., 1992. Micrometer-sized glass spheres in Apollo 16 soil 61181 - Implications for impact volatilization and condensation. In: Lunar and Planetary Science Conference Proceedings, vol. 22, pp. 137–141.
Keller, L.P., Mckay, D.S., 1993. Discovery of vapor deposits in the lunar regolith. Science 261 (5126), 1305–1307.
Keller, L.P., McKay, D.S., 1997. The nature and origin of rims on lunar soil grains. Geochim. Cosmochim. Acta 61 (11), 2331–2341.
Kelly, R., Rowson, N., 1995. Microwave reduction of oxidised ilmenite concentrates. Miner. Eng. 8 (11), 1427–1438.
Liu, Y., Taylor, L.A., Thompson, J.R., Schnare, D.W., Park, J.S., 2007. Unique properties of lunar impact glass: Nanophase metallic Fe synthesis. Am. Mineral. 92 (8–9), 1420–1427.
Liu, D., Zhang, Y., Zhang, G., Liu, B., Ren, X., Xu, R., Li, C., 2020. An Empirical Model to Estimate Abundance of Nanophase Metallic Iron (npFe0) in Lunar Soils. Remote Sensing 12 (6), 1047.
Makhova, M., Bocharova, I., Mishchenko, E., Kovalenko, V., 1989. Glass fiber from rock. Glass Ceram. 46 (9), 374–376.
Morris, R.V., 1980. Origins and size distribution of metallic iron in the lunar regolith. In: Lunar and Planetary Science Conference, pp. 747–749.
Nagata, T., Ishikawa, Y., Kinoshita, H., Kono, M., Syono, Y., Fisher, R., 1970. Magnetic properties and natural remanent magnetization of lunar materials. Geochim. Cosmochim. Acta Suppl. 1, 2325–2340.
Pieters, C.M., Fischer, E.M., 1993. Optical Effects of Space Weathering: The Role of the Finest Fraction. J. Geophys. Res. 98 (20), 20817–20824.
Rice, E., Rosenberg, S., Musbah, O., Hermes, P., Bemowski, P., 1996. Carbothermal reduction of lunar materials for oxygen production on the moon. In: 34th Aerospace Sciences Meeting and Exhibit, p. 487.
Sen, S., Butts, D., Ray, C.S., Thompson, G.B., Morris, R.A., O'Dell, J.S., 2011. Production of high fidelity lunar agglutinate simulant. Adv. Space Res. 47 (11), 1912–1921.
Sen, S., Butts, D., O'Dell, J., Ray, C., 2010. Plasma processing of lunar regolith simulant for oxygen and glass production. In: Earth and Space 2010: Engineering, Science, Construction, and Operations in Challenging Environments, pp. 1343–1352.
Tang, H., Wang, S., Li, X., 2012. Simulation of nanophase iron production in lunar space weathering. Planet. Space Sci. 60 (1), 322–327.
Tang, H., Li, X., Zhang, S., Wang, S., Liu, J., Li, S., Li, Y., Wu, Y., 2017. A lunar dust simulant: CLDS-i. Adv. Space Res. 59 (4), 1156–1160.
Thompson, M.S., Zega, T.J., Keane, J.T., Becerra, P., Byrne, S., 2015. The oxidation state of fe nanoparticles in lunar soil: Implications for space weathering processes. Lunar and Planetary Science Conference (1832), 2932.
Wang, Y., Yuan, Z., 2006. Reductive kinetics of the reaction between a natural ilmenite and carbon. Int. J. Miner. Process. 81 (3), 133–140.